J Appl Electrochem (2010) 40:809–819
DOI 10.1007/s10800-009-0064-3

ORIGINAL PAPER

Response of a proton exchange membrane fuel cell to a sinusoidal current load

Helge Weydahl · Magnus S. Thomassen · Børre T. Børresen · Steffen Møller-Holst

Received: 17 October 2008 / Accepted: 23 December 2009 / Published online: 16 January 2010

Abstract The load-following capability of a proton exchange membrane fuel cell was studied by measuring the cell voltage response to a sinusoidal current load with large amplitude and varying frequency. A mathematical model was developed, incorporating mass transport and capacitive effects as well as the membrane resistance. The model was capable of separating the faradaic and capacitive currents and predicting the observed hysteresis. At frequencies of the sinusoidal current load below 1 Hz, no appreciable hysteresis in the polarisation curve was observed. When increasing the frequency above 1 Hz, a hysteresis appeared at current densities below 0.2 A cm^{-2}. The model related this hysteresis to capacitive effects. When using air as the cathode feed, hysteresis in the current density range 0.5 A cm^{-2} and higher appeared above 1 Hz compared to 100 Hz for pure oxygen. The model revealed that hysteresis observed in this current density range was caused by oxygen transport limitations.

H. Weydahl · B. T. Børresen
Department of Materials Science and Engineering, NTNU, 7491 Trondheim, Norway

M. S. Thomassen · S. Møller-Holst (✉)
SINTEF Materials and Chemistry, 7465 Trondheim, Norway
e-mail: Steffen.Moller-Holst@sintef.no

Present Address:
H. Weydahl
Prototech AS, P.O. Box 6034, Postterminalen, 5892 Bergen, Norway

Present Address:
B. T. Børresen
Statoil ASA, 7005 Trondheim, Norway

Keywords Proton exchange membrane fuel cells · Load-following · Dynamic behaviour · Transient model

List of symbols

Roman letters

A	Electrode area (cm^2)
b_c	Fitting parameter for the concentration overvoltage (V)
b_k	Tafel slope (V)
C	Cathode capacitance (F cm^{-2})
c_g	Molar concentration of an ideal gas at a given temperature and 1 bar (mol cm^{-3} bar^{-1})
c_i	Concentration of species i (mol cm^{-3})
c_i^0	Concentration of species i at a reference condition (mol cm^{-3})
$D_i^{'}$	Effective gas diffusivity of species i (cm^2 s^{-1})
e^-	Electron
E	Electronic potential of an electronically conductive solid phase (V)
E_{cell}	Total cell voltage (V)
E^{rev}	Reversible electrode potential at the given conditions (V)
E^0	Theoretical open circuit potential at standard conditions (V)
E_0	Constant voltage fitting parameter (V)
f	Frequency (Hz)
F	Faraday's constant (C mol^{-1})
i	Local current density (A cm^{-2})
i_0	Exchange current density (A cm^{-2})
i_d	Capacitive current density (A cm^{-2})
i_{far}	Faradaic current density (A cm^{-2})
i_{int}	Internal current density due to hydrogen cross-over (A cm^{-2})
i_{lim}	Limiting current density (A cm^{-2})
M_i	Symbol for the chemical formula of species i

m_i Reaction order of species i
N_i Molar flux of species i (mol cm^{-2} s^{-1})
n Number of electrons transferred
p_i Partial pressure of species i (bar)
R Ideal gas constant (J K^{-1}mol^{-1})
R_{mem} Membrane resistance (Ω)
R_i^e Electrochemical reaction rate per unit volume for species i (mol cm^{-3}s^{-1})
s_i Stoichiometric coefficient of species i
T Absolute temperature (K)
t Time (s)
x Distance from the membrane/cathode catalyst interface (cm)
z_i Charge number of species i

Greek letters

α_a Apparent anodic transfer coefficient
α_c Apparent cathodic transfer coefficient
δ Thickness of Nernstian diffusion layer (cm)
η Local overpotential (V)
Φ Electronic potential of an ionically conductive phase (V)

Superscripts

0 Reference conditions
rev Reversible conditions
ss Steady state

Subscripts

CC Current collector
CCL Cathode catalyst layer
e Electrochemical
i Species i
mem Membrane
O_2 Oxygen
ox Oxidised species
red Reduced species

1 Introduction

Among the various fuel cell technologies, the proton exchange membrane fuel cell (PEMFC) is considered the most promising replacement of internal combustion engines [1]. For commercial success in automotive vehicles and other applications with rapidly varying power demands, the load-following capability of the PEMFC is of high importance [2]. In fuel cell systems for dynamic power demands, energy buffers such as batteries and capacitors are often added to avoid deviations between required and supplied power. However, if the PEMFC is sufficiently fast to follow also a time-varying load, such components may become redundant, giving a cheaper and more compact energy conversion system.

The ability of a PEMFC to follow a varying power demand is determined by how fast each process in the PEMFC responds to a load change. The initial response is determined by the ohmic potential drop, which is instantaneous, and capacitive discharge of the electrode. An increased power output also causes a higher consumption rate of reactant gases in the catalyst layer. This causes a redistribution of reactant gases in the catalyst layers, gas diffusion layers (GDLs) and gas channels of the PEMFC, taking place on a time scale of a few seconds [3–6]. A higher power output also increases water production at the cathode. Gaseous water represents a diffusion barrier for oxygen, and liquid water may cover active sites in the catalyst layer and block gas transport [3, 7]. Liquid water also affects the water balance of the membrane, giving variations in membrane conductivity on a time scale of seconds to several minutes [6, 8–12]. Changes in cell temperature take place on a time scale of minutes [13–15], but rapid local temperature increases may occur. Dynamic changes on a time scale of seconds and slower can be handled by a well-designed PEMFC controller ensuring stable power output even though cell performance varies. Faster changes in the power output, such as those due to ohmic drop, capacitive discharge and redistribution of reactant gases, cannot be controlled in the same manner. These processes must therefore be characterised so that design criteria for a suitable buffer system can be determined.

The load-following capability of PEMFCs has been addressed in a number of papers. Jones et al. [16] and Hottinen et al. [17] evaluated the ability of a PEMFC to sustain current pulses appearing in portable electronics, but did not report high-resolution measurements of the rapid cell voltage response. Ziegler et al. [18] modelled the response in PEMFC current to slow voltage sweeps at constant sweep rate. Hysteresis in current was attributed to water accumulation in the cathode GDL. Hamelin et al. [19] and Amphlett et al. [20] measured the cell voltage response of PEMFC stacks to a step in current. These studies revealed the initial rapid response of PEMFCs. Williams et al. [21] investigated the dynamic response of a PEMFC stack in interaction with a DC/DC converter, demonstrating the feasibility of this system in a load-following mode. The use of capacitors to reduce the ripple current from power converters was addressed by Schenck et al. [22]. Both these latter studies focused on the dynamic response on a stack level and did not address the load-following capability on a single cell level.

According to Fourier series theory, any periodic function can be represented by a sum of sine and cosine functions with different frequencies and amplitudes. The ability of fuel cells to follow any periodic load profile can therefore be revealed by measuring the fuel cell response to

a sinusoidal load with varying mean value, frequency and amplitude. This approach is different from the well-known electrochemical impedance spectroscopy (EIS) technique where a sinusoidal perturbation with *small* amplitude is applied [23]. By using a small amplitude, linear theory can be used to analyse response data. The EIS technique separates and quantifies processes with different response times at the chosen steady-state operating point. However, it does not capture how these processes change during the transition from one steady-state operating point to another. By using a *large* amplitude perturbation, the fuel cell response to finite load changes is captured, but linear theory can no longer be applied to analyse response data. Still, this technique can provide qualitative information on the load-following capability of the fuel cell.

In this study, we apply a large-amplitude sinusoidal current load to a single PEMFC and measure the cell voltage response for varying frequencies of the input current. This way, the load-following capability in the full operating range of the PEMFC was mapped. Current was chosen as the controlled variable since a forced rapid increase in cell voltage may lead to reversal of the current [24]. The objective of this study was to determine how fast changes the PEMFC could follow, at which frequency the transient and steady-state response deviate, the characteristic shape of the deviation and its relation to physical processes. In order to address the effect of mass transport on the transient response, measurements were carried out using both oxygen and air as cathode gases. Furthermore, a simple mathematical model was applied to interpret the experimental results and to separate the capacitive and faradaic contributions to the PEMFC voltage response.

2 Experimental

2.1 Hardware and operating conditions

A membrane electrode assembly (MEA) from W. L. Gore & Associates (PRI-MEA® MEA, Cleo Series 58, membrane thickness 18 μm, 0.4 mg cm^{-2} Pt on both anode and cathode) was sandwiched between two GDLs from E-TEK (ELAT® carbon only). The geometric electrode area was 6.25 cm^2. The MEA and GDLs were mounted in a fuel cell housing from ElectroChem (EFC05-01SP-REF) with triple serpentine flow channels.

The anode was supplied with a constant gas flow of hydrogen (99.999% purity) and the cathode with oxygen (99.5% purity) or synthetic air (79% N_2 and 21% O_2 at 99.999% purity). To avoid any effects of fuel starvation, both gases were supplied in excess so that consumption never exceeded 20%. The gases were humidified in separate sparge bottles. To ensure an equal and even temperature, both the PEMFC and sparge bottles were placed in a heating cabinet from Termaks (TS8136) at a temperature of 45 °C. The temperature of the cathode housing was monitored by a thermocouple from Omega®, and the operating temperature was 46 ± 3 °C and 44 ± 1 °C during experiments with pure oxygen and air, respectively. During the EIS measurements with pure oxygen and air, the temperature was 47 ± 5 °C and 50 ± 5 °C, respectively. These temperature variations were assumed not to affect our results significantly.

2.2 Sinusoidal current load

A sinusoidal current load was realised using a Wenking STP 84 Standard Potentiostat from Bank Elektronik. This potentiostat is designed for potentiostatic operation only, but by controlling the voltage across a shunt resistor (ARCOL HS200 R47, 0.47 Ω, 50 W power resistor), galvanostatic operation was obtained. It was verified that the resistance of the power resistor was constant throughout the measured current range.

The circuit diagram of the experimental set-up is shown in Fig. 1. A 15 MHz synthesised function generator from Yokogawa (FG300) produced the sinusoidal control signal for the potentiostat. Separate tests verified that the potentiostat was able to produce sinusoidal currents in the applied range. The technical capacity of the potentiostat limited the peak value and frequency of the applied current to 5.5 A and 1 kHz, respectively.

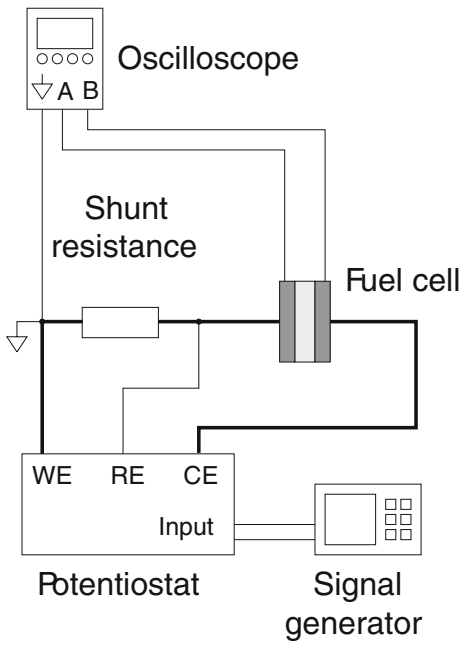

Fig. 1 Experimental set-up for the sinusoidal current load measurements

A digital oscilloscope from Pico® Technology Ltd. (ADC-212) monitored the fuel cell voltage and the voltage across the shunt resistor. The relation between shunt resistor voltage and current was found by comparing oscilloscope data with current readouts from the potentiostat. The shunt resistor was connected directly to the fuel cell cathode end plate using a thick bronze connector, ensuring minimal resistance between shunt resistor and fuel cell cathode.

The PEMFC was allowed to settle for at least two time periods at each frequency before the voltage response was recorded, ensuring that the "steady-state" periodic response was established.

2.3 Electrochemical measurements

Electrochemical impedance spectroscopy (EIS) was performed on a two-electrode setup (full cell) using an IM6e electrochemical workstation and PP200 add-on module from ZAHNER® elektrik. An AC signal with amplitude 2.5 mV and a frequency range from 100 kHz to 100 mHz was applied. The impedance was measured at various steady-state cell voltages to see how the impedance response changed with cell voltage. The cell voltage was allowed to settle for at least 1 min at each potential before the impedance spectrum was recorded. Polarisation curves were obtained with the ZAHNER® equipment using a sweep rate of 1 mV s^{-1}.

3 Mathematical model

A simple, one-dimensional and transient mathematical model of the PEMFC was developed as a tool for interpretation of the experimental results. The model is based on the classical porous electrode model presented by Newman [25] and incorporates mass transport and capacitive effects in the cathode as well as the ionic resistance in the ionomer membrane. In the model, it is assumed that the influence of the fuel cell anode can be neglected. As the fuel cell was operated at a rather low temperature of 45 °C, the amount of water vapour was relatively low. We therefore neglect the net production and transport of water vapour in this model, but include the effect of water vapour as a diffusion barrier for oxygen. Therefore, oxygen is the only species included in the transport equations.

3.1 Governing equations

The equation of continuity for species i can be written in the general form

$$\frac{\partial c_i}{\partial t} = -\frac{\partial}{\partial x} N_i + R_i^e \tag{1}$$

where t is time, x is the distance from the membrane/cathode catalyst interface, c_i and N_i refer to the concentration and molar flux of species i, respectively, and R_i^e indicates the electrochemical reaction rate of species i per unit volume. As stated above, the model only includes this equation for oxygen. Also, the reaction rate of oxygen in the GDL is zero. The equation is solved between $x = 0$ and $x = \delta$ where δ is the thickness of the Nernstian diffusion layer.

For this simple model, it is assumed that Fick's law for binary diffusion can be used as the flux expression, N_i,

$$N_i = -D_i^{'} \frac{\partial}{\partial x} c_i = -D_i^{'} c_g \frac{\partial}{\partial x} p_i \tag{2}$$

where $D_i^{'}$ is the effective gas diffusivity, c_g is the molar concentration of an ideal gas per bar at the given temperature and p_i is the partial pressure of species i measured in bar.

The stoichiometric coefficient is given by expressing an electrochemical reaction in the form

$$\sum_i s_i M_i^{z_i} \rightarrow n\mathrm{e}^- \tag{3}$$

where S_i is the stoichiometric coefficient of species i, M_i is a symbol for the chemical formula of species i, n denotes the number of electrons transferred in the reaction and z_i is the charge number of species i.

The faradaic current density, i_{far}, can be described by the Butler–Volmer equation

$$i_{\mathrm{far}} = i_0 \left[\prod_{\mathrm{red}} \left(\frac{c_{\mathrm{red}}}{c_{\mathrm{red}}^0} \right)^{m_{\mathrm{red}}} \exp\left(\frac{\alpha_a n F \eta}{RT} \right) - \prod_{\mathrm{ox}} \left(\frac{c_{\mathrm{ox}}}{c_{\mathrm{ox}}^0} \right)^{m_{\mathrm{ox}}} \exp\left(\frac{-\alpha_c n F \eta}{RT} \right) \right] \tag{4}$$

where i_0 is the exchange current density, c_{red} and c_{ox} are the concentrations of the anodic and cathodic reactants, c_{red}^0 and c_{ox}^0 are the concentrations of the anodic and cathodic reactants at a chosen reference condition, m_{red} and m_{ox} are the reaction orders of the anodic and cathodic reactants, α_a and α_c are the apparent anodic and cathodic transfer coefficients, F is Faraday's constant, R is the ideal gas constant, T is the absolute temperature and η is the local overpotential. In our model, we neglect the contribution by the anodic terms giving the following simplified expression for Eq. 4

$$i_{\mathrm{far}} = -i_0 \left(\frac{c_{\mathrm{O_2}}}{c_{\mathrm{O_2}}^0} \right)^{m_{\mathrm{O_2}}} \exp\left(\frac{-\alpha_c n F \eta}{RT} \right) \tag{5}$$

The capacitive current density, i_d, charging/discharging the interfacial electrochemical double layer of the cathode is defined as

$$i_d = C\frac{\partial \eta}{\partial t} \tag{6}$$

where C is the capacitance of the cathode.

The faradaic and capacitive current density give the total current density which is equal to the applied sinusoidal current load used in the experiments

$$i = i_{\text{far}} + i_d = (0.41 + 0.40\sin(2\pi ft)) \tag{7}$$

with unit A cm^{-2} where f is the frequency of the sinusoidal current load.

The local overpotential in the cathode catalyst layer is given by

$$\eta = E - \Phi - E^{\text{rev}} \tag{8}$$

where E is the electronic potential of an electronically conductive solid phase, Φ is the electronic potential of an ionically conductive phase and E^{rev} is the reversible electrode potential at the given conditions given by

$$E^{\text{rev}} = E^0 - \frac{RT}{nF}\sum_i s_i \ln\left(\frac{c_i}{c_i^0}\right) \tag{9}$$

where E^0 is the theoretical open circuit potential at standard conditions.

The electronic potential can be arbitrarily fixed either at the anode or cathode current collector. Setting the value at the anode to zero and neglecting the gradient in electronic potential between the cathode catalyst layer and the cathode current collector, we get

$$E = E_{\text{cell}} \tag{10}$$

where E_{cell} is the total cell voltage.

In this model, we assume that the ionic resistance in the ionomer membrane can be represented by Ohm's law. Also, since the potential gradient in the anode has been neglected in this model, the electronic potential at the anode/membrane interface can be arbitrarily fixed. Setting the membrane potential at this boundary to zero gives

$$\Phi = iAR_{\text{mem}} \tag{11}$$

where A is the electrode area of the single cell and R_{mem} the total resistance of the membrane.

3.2 Boundary and initial conditions

Oxygen is consumed at the membrane/cathode catalyst interface, giving the following boundary condition for Eq. 1

$$N_{\text{O}_2}|_{\text{CCL}} = -\frac{s_{\text{O}_2} i_{\text{far}}}{nF} \tag{12}$$

CCL denotes cathode catalyst layer and refers to the membrane/cathode catalyst interface.

The second boundary condition is obtained by assuming a uniform distribution of gases in the cathode gas channels. Thus, the partial pressure of oxygen at the interface between the cathode GDL and the cathode gas channel can be set to

$$p_{\text{O}_2}|_{\text{CC}} = p^0 \tag{13}$$

for the PEMFC operated on pure oxygen and

$$p_{\text{O}_2}|_{\text{CC}} = 0.21p^0 \tag{14}$$

for the PEMFC operated on air. Here, CC denotes current collector and refers to the cathode GDL/gas channel interface.

The initial conditions are set to the reference conditions of the cathode gas. i.e.

$$p_{\text{O}_2}(t=0) = p^0 \tag{15}$$

for the PEMFC operated on pure oxygen and

$$p_{\text{O}_2}(t=0) = 0.21p^0 \tag{16}$$

for the PEMFC operated on air.

3.3 Model parameters

The model was developed to explain the shape of the voltage response of the PEMFC for the different frequencies of the current perturbation applied. In order to make the output data from the mathematical model as representative as possible for the fuel cell under study, a major part of the model parameters was determined by curve fitting to an empirical equation representing the steady-state polarisation response of the PEMFC. Several empirical equations for curve fitting of fuel cell polarisation curves have been suggested [26–29]. All of the fitting equations presented in these papers consist of a constant cell voltage fitting parameter, a logarithmic term representing the charge transfer overvoltage and one or two terms describing the non-ohmic overvoltage due to mass transport limitations (also know as the concentration overvoltage). By using elements from the fitting equations by Kim et al. [27] and Fraser et al. [26], the following empirical fitting equation was developed for extracting model parameters from the steady-state polarisation curves:

$$E_{\text{cell}}^{\text{ss}} = E_0 - (i + i_{\text{int}})R_{\text{mem}} - b_k\left(\frac{i + i_{\text{int}}}{i_0}\right) + b_c \ln\left(1 - \frac{i + i_{\text{int}}}{i_{\text{lim}}}\right) \tag{17}$$

where $E_{\text{cell}}^{\text{ss}}$ is the total fuel cell voltage at steady state, E_0 is the constant voltage fitting parameter, b_k the Tafel slope, i_{int} the internal current flowing due to hydrogen cross-over, i_{lim} the limiting current density and b_c the fitting parameter for the concentration overvoltage.

The recorded polarisation curves were fitted to Eq. 17 using the non-linear curve fitting tool in Origin 7.5. The

Table 1 Model parameters obtained from curve fitting to Eq. 17. C was obtained from EIS measurements

Symbol Unit	E_0 V	R_{mem} Ω	i_{int} A cm^{-2}	b_k V	i_0 A cm^{-2}	b_c V	i_{lim} A cm^{-2}	C F cm^{-2}
H_2/O_2	1.16	0.07	0.0025	0.032	3.57×10^{-6}	0.13	4.37	0.030
H_2/air	1.15	0.08	0.0042	0.030	1.85×10^{-6}	0.10	1.28	0.035

resulting parameters obtained for use in the mathematical model are given in Table 1.

The suggested model also includes the capacitive charging/discharging of the cathode. To obtain the capacitance of the PEMFC, a series of EIS measurements were carried out. The resulting impedance responses were subsequently fitted to a widely employed equivalent circuit for a PEMFC [30–36] using the non-linear least squares technique in the ZSimpWin software. The obtained values for the electrode capacitance are included in Table 1. These are in the same range as reported by, e.g. Liu et al. [37]. The observed electrode capacitance is mainly due to the potential dependent pseudocapacitance of platinum.

The same value for the effective gas diffusivity of oxygen was used both for the case with pure oxygen and with air, but the values used for the thickness of the Nernstian diffusion layer were different for the two cases. These values were estimated using the value for i_{lim} found from Eq. 17 using the following relation

$$\delta = \frac{c^0_{O_2} D'_{O_2} nF}{i_{lim}} \tag{18}$$

Table 2 Model parameters

Symbol	Value	Unit
A	6.25	cm^2
c_g	4.03×10^{-5}	mol cm^{-3} bar^{-1}
$c^0_{O_2}$ (oxygen)	4.03×10^{-5}	mol cm^{-3}
$c^0_{O_2}$ (air)	0.847×10^{-5}	mol cm^{-3}
D'_{O_2}	0.1	cm^2 s^{-1}
δ (oxygen)	0.356	cm
δ (air)	0.255	cm
F	96,485	C mol^{-1}
m_{O_2}	1	
m_{H_2O}	2	
n	4	
p^0	1	bar
R	8.3145	JK^{-1} mol^{-1}
s_{O_2}	1	
s_{H_2O}	−2	
T	318	K

Here, $c^0_{O_2}$, i_{lim} and hence also δ have different values for oxygen and air.

The fitting parameter for the Tafel slope, b_k, is assumed to be equal to $RT/\alpha_C nF$ and used in the Butler–Volmer equation (Eq. 5). All remaining parameters used in the mathematical model are listed in Table 2.

3.4 Method of solution

The model equations are highly coupled and non-linear and a numerical solution was required. The finite element method program Comsol Multiphysics® 3.5a with the chemical engineering toolbox from Comsol AB was employed to solve the equations. A multiphysics model incorporating two application modes and two dependent variables was created and a transient solver was used to solve the model. The model was run until a steady-state response to the sinusoidal current perturbation was observed.

4 Results and discussion

4.1 Response of the PEMFC to a sinusoidal current load

A sinusoidal current load was applied to a PEMFC supplied with pure oxygen and hydrogen. The mean value (0.41 A cm^{-2}) and amplitude (0.40 A cm^{-2}) of the sinusoidal current were kept constant while the frequency was varied between 0.1 Hz and 1 kHz. Measurements were repeated replacing oxygen with synthetic air as cathode gas. Figure 2 shows the steady-state polarisation curves and the sinusoidal response at various frequencies in V-i diagrams for the PEMFC operated on both pure oxygen and synthetic air. For the PEMFC operating on pure oxygen, cell voltage hysteresis appeared at frequencies above 0.1 Hz at low current densities (<0.2 A cm^{-2}). As frequency increased, hysteresis was seen also for higher current densities (>0.5 A cm^{-2}), and at 100 Hz hysteresis was present all the way up to the maximum current density of 0.81 A cm^{-2}. At 100 Hz the hysteresis of oxygen and air was almost identical in shape, only shifted along the abscissa by approx. 0.06 V. At 1 kHz, hysteresis was less pronounced and the response approached a straight line.

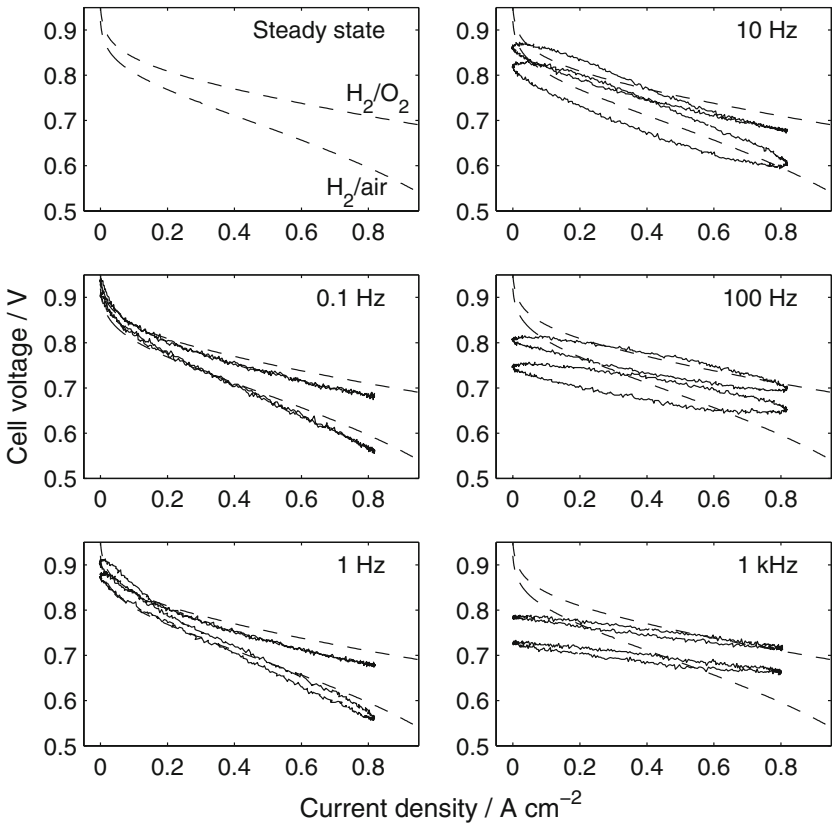

Fig. 2 The PEMFC voltage responses to a sinusoidal current (mean value 0.41 A cm^{-2} and amplitude 0.40 A cm^{-2}) at various frequencies (0.1 Hz–1 kHz) with the steady-state polarisation curve (*dashed lines*) obtained at a sweep rate of 1 mV s^{-1} with hydrogen as anode gas. The *solid lines* in each diagram show the voltage response of the PEMFC operated with pure oxygen (*upper line*) and synthetic air (*lower line*) as cathode feed gas. Time increases clockwise around the cell voltage loops

For cells operating on synthetic air, hysteresis was found for all current densities at frequencies higher than 0.1 Hz. The hysteresis for current densities 0.5 A cm^{-2} and higher appeared above 1 Hz compared to 100 Hz when using oxygen as cathode feed. The load-following capability of the PEMFC was thus reduced (hysteresis was more pronounced) when using air as cathode feed. The more pronounced hysteresis for air is related to diffusion limitations as will be further discussed in Sect. 4.3.

For both air and oxygen, the sinusoidal voltage response was somewhat lower than that of the steady-state polarisation curve at higher current densities. This is best seen at the frequency of 0.1 Hz and is assumed to be related to differences in cell temperature. During sinusoidal current variations, the mean cell current of 0.41 A cm^{-2} corresponds to less heat dissipation than what is experienced during steady-state operation at higher current densities.

4.2 Modelling results

Modelling results for the PEMFC operated on pure hydrogen and oxygen and hydrogen/air are compared to the experimental results in Fig. 3. The onset and shape of the measured hysteresis is reproduced with satisfactory precision, even though the applied model is rather simple. There is a discrepancy between the experimental and modelled cell voltage values, especially at low current densities. A more sophisticated model would probably reduce this discrepancy, but Fig. 3 still confirms that the applied model (described in Sect. 3) constitutes an adequate tool for representing and interpreting the dynamic behaviour of the PEMFC.

4.3 Separation of hysteresis into capacitive and mass transport contributions

With the adequacy of the applied model being confirmed in Fig. 3, the model was used to determine which processes were responsible for the hysteresis in the various frequency and current density domains. Since the model includes both faradaic reactions and charging of the electrode capacitance, the contribution to the overall cell current from each of these processes as a function of frequency and total current density was easily extracted from Eqs. 5 and 6. In Fig. 4, the capacitive and faradaic contributions to the total current density in our model are compared. At 0.1 Hz, nearly all current was found to be faradaic. As the frequency increases, the capacitive contribution to the total current increases. The capacitive current contribution is both positive and negative and gives hysteresis in the total current. The capacitive current was, as shown in Eq. 6, proportional to the change of the cell voltage. The voltage change is largest at low current

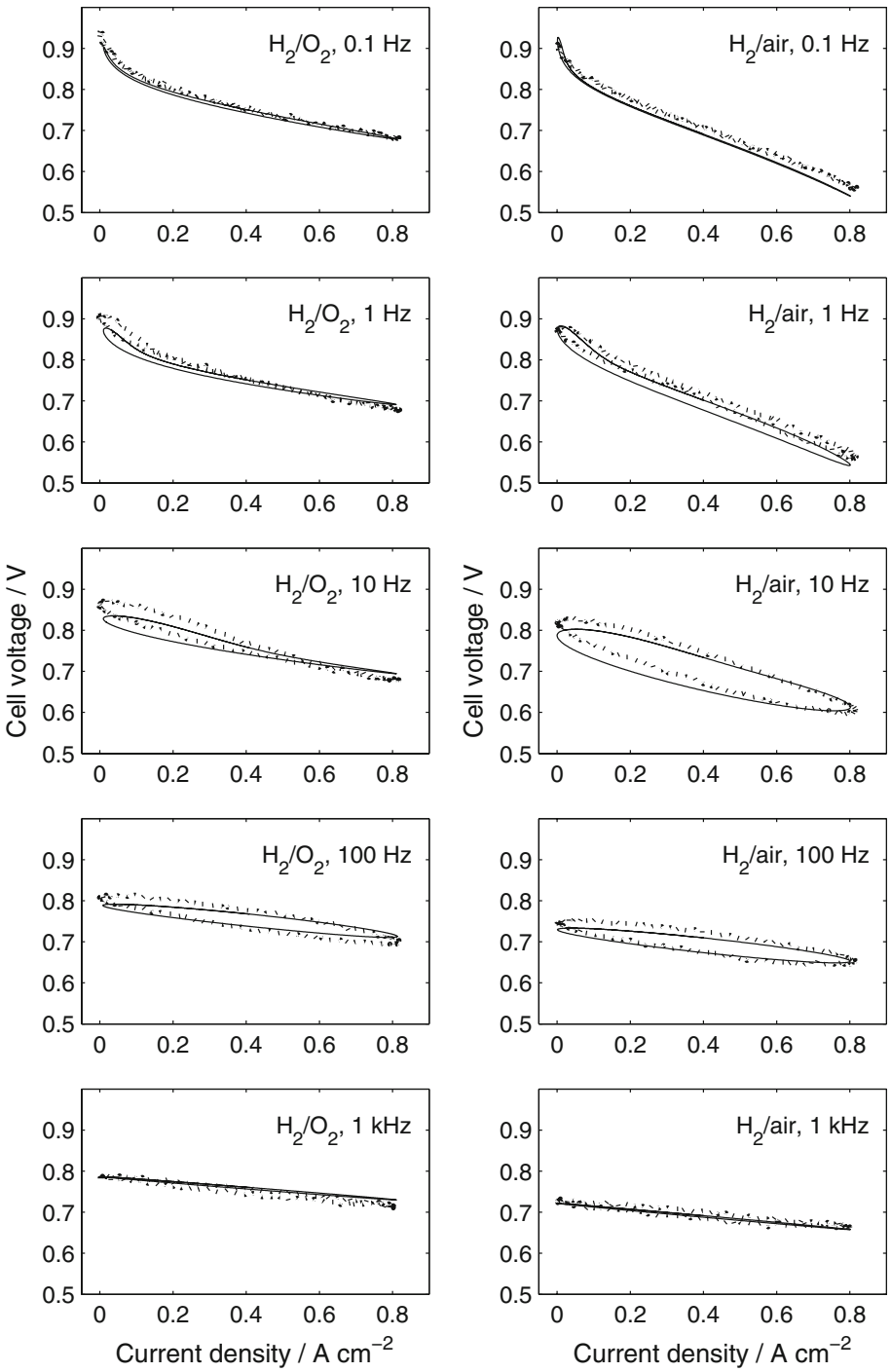

Fig. 3 Comparison of modelling (*solid lines*) and experimental results (*dotted lines*) for the PEMFC voltage response to a sinusoidal current (mean value 0.41 A cm^{-2} and amplitude 0.40 A cm^{-2}). The cell was operated on pure hydrogen and oxygen (*left column*) and hydrogen/air (*right column*). Time increases clockwise around the cell voltage loops

densities, consequently hysteresis in the capacitive current appears first at low current densities.

At 10 Hz we also observe hysteresis in the faradaic current, which can be ascribed to a higher oxygen concentration in the cathode catalyst layer at increasing current than at decreasing current. As the frequency increases, the hysteresis first increases, and then decreases. At 100 Hz, both the faradaic and capacitive current contribute comparably to the overall voltage hysteresis. At 1 kHz, the faradaic contribution oscillates with only a small amplitude around the mean current density, and the capacitive contribution is responsible for the main part of the oscillations in total current density.

Comparison of the modelling results with oxygen and air as cathode gas (Fig. 4) shows one important difference: Due to the larger mass transport limitations when air is used, hysteresis in the faradaic current contribution is significant and pronounced at higher current densities already at 1 Hz. This is caused by the higher mass transport when operating

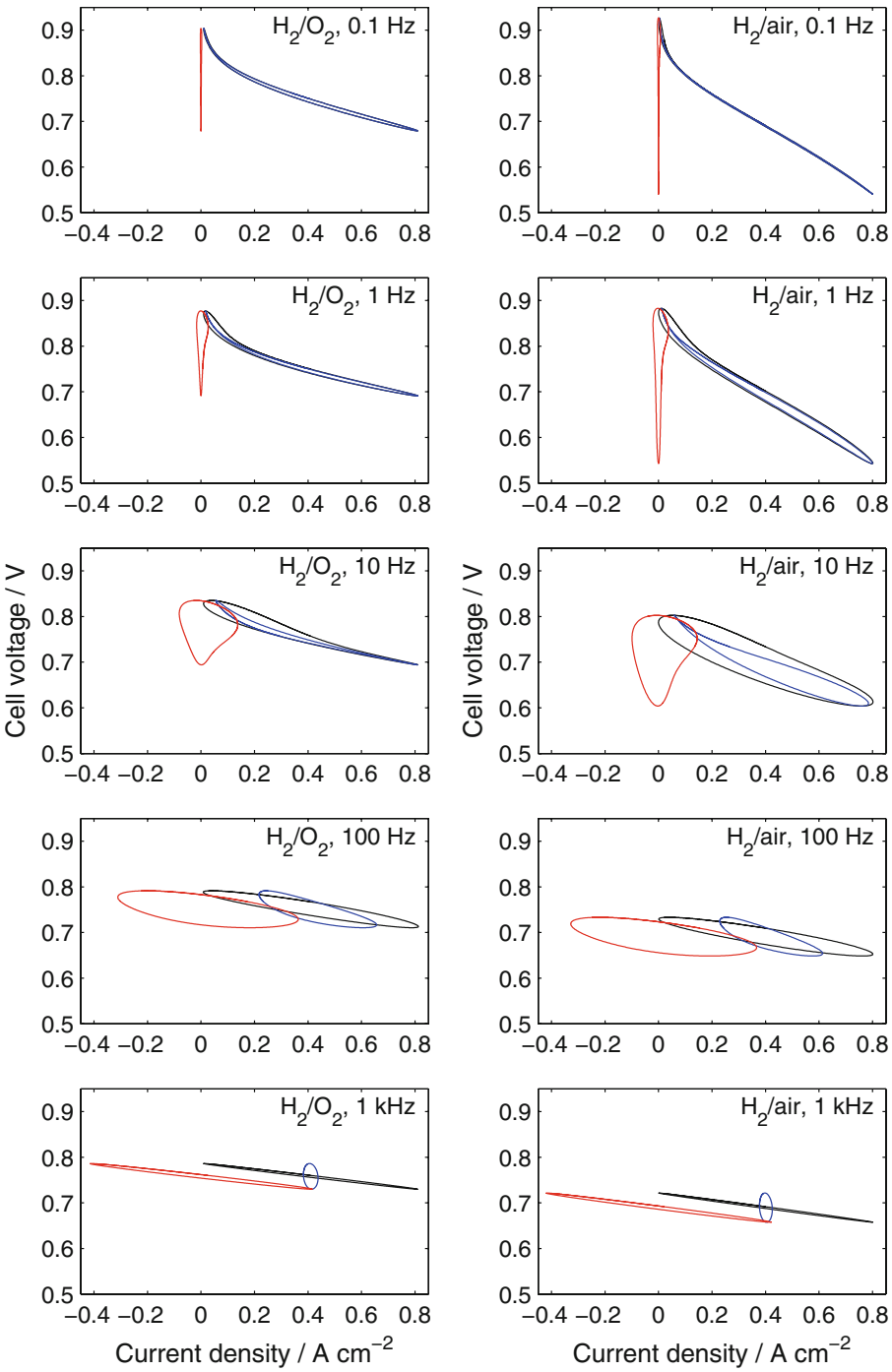

Fig. 4 Contribution of faradaic (*blue line*) and capacitive (*red line*) current density to the total current density (*black line*) for the PEMFC operated on pure hydrogen and oxygen (*left column*) and hydrogen/air (*right column*). The separation is based on the model described in Sect. 3 (Eqs. 5 and 6)

on air, giving larger oscillations in the oxygen concentration at the cathode. The hysteresis at higher current densities measured at 1 and 10 Hz can therefore be ascribed to mass transport limitations in the cathode.

4.4 Implications for further development of PEMFCs

The PEMFC's very rapid response to load changes constitutes one of the major advantages of this technology, making it viable for a series of applications. This study has, however, revealed that both capacitive and mass limiting processes contribute to significant hysteresis effects when the PEMFC is subject to sinusoidal load changes. With this increased insight into the dynamics and load-following capabilities, and the corresponding model showing good agreement with experimental results, a sensitivity analysis with respect to model parameters' influence on dynamics is feasible. Quantification of how changes in, e.g. the oxygen

diffusion coefficient or electrode capacitance influence the hysteresis may eventually lead to a description of how a PEMFC should be made to enhance load-following capabilities. Thus, an optimal electrode morphology may be determined for PEMFC applications with certain requirements on the dynamic response.

The question of how the electrode capacitance affects the PEMFC durability then arises. Assuming a fast varying power demand, requiring an equivalent response from the fuel cell will, if no capacitive behaviour is present, force the faradaic processes according to the power demand. Large variations in the electrode potential and local temperature increase due to mass and heat transfer limitations may occur, with an expected negative effect on cell life-time. In severe cases, the transport of reactants to the electrocatalysts under rapidly changing power demand can be insufficient, causing unwanted side reactions such as carbon or platinum corrosion or cell reversal to occur. With an intrinsic capacitive behaviour of the electrode, the presented model shows that the initial 10 ms of a large load change may be handled by the capacitive properties of the electrode, leaving more time for the faradaic reactions to catch up with the power demand. From this perspective, a high electrode capacitance can shield the cell from large forced changes in faradaic current, give smoother fuel cell operation, and hence contribute to increased cell life-time.

5 Conclusion

The load-following capability of a PEMFC was studied by measuring the cell voltage response to a sinusoidal current load with varying frequency and interpreting the results using a simple mathematical model. The mathematical model was able to describe the observed voltage response to the sinusoidal current loads at selected frequencies for both oxygen and air operation. The model also facilitated separation of the faradaic and capacitive contributions to the hysteresis.

At frequencies of the sinusoidal current load below 1 Hz, no appreciable hysteresis in the polarisation curve was observed. However, increasing the frequency above 1 Hz, a hysteresis appeared at low current densities. A more detailed analysis using the developed model showed that this hysteresis was caused by capacitive effects.

The PEMFC operated on hydrogen and oxygen showed better load-following capabilities (smaller hysteresis) than the PEMFC operated on hydrogen and air. Explicitly it was observed that when using air as the cathode feed, hysteresis in the current density range 0.5 A cm^{-2} and higher appeared at 1 Hz as compared to 100 Hz for pure oxygen. The model revealed that hysteresis observed in this current density range was caused by oxygen transport limitations.

The reported measurements and model analysis showed that the intrinsic capacitance of the PEMFC electrode can shield the cell from large forced changes in faradaic current occurring on a time scale of 10 ms. Thus, the electrode capacitance may have a positive effect on the lifetime of the cell. The long-term effects of a fluctuating load on the overall PEMFC performance should be further investigated.

Acknowledgements The Research Council of Norway and Aker Kværner Power & Automation Systems AS are kindly acknowledged for financial support. Prototech, Statoil and SINTEF are acknowledged for supporting the writing of this paper.

References

1. Pukrushpan JT, Peng H, Stefanopoulou AG (2004) J Dyn Syst—T ASME 126:14
2. Ahluwalia RK, Wang X (2005) J Power Sources 139:152
3. Natarajan D, Nguyen TV (2001) J Electrochem Soc 148:A1324
4. Brett DJL, Atkins S, Brandon NP et al (2001) Electrochem Commun 3:628
5. Stockie JM, Promislow K, Wetton BR (2003) Int J Numer Methods Fluids 41:577
6. Wang Y, Wang C-Y (2005) Electrochim Acta 50:1307
7. He W, Lin G, Nguyen TV (2003) AIChE J 49:3221
8. Okada T, Xie G, Tanabe Y (1996) J Electroanal Chem 413:49
9. Friede W, Raël S, Davat B (2004) IEEE T Power Electron 19:1234
10. Chia E-SJ, Benziger JB, Kevrekidis IG (2004) AIChE J 50:2320
11. Chen F, Su Y, Soong C et al (2004) J Electroanal Chem 566:85
12. Chen F, Chu H-S, Soong C-Y et al (2004) J Power Sources 140:243
13. Amphlett JC, Mann RF, Peppley BA et al (1996) J Power Sources 61:183
14. Shan Y, Choe S-Y (2005) J Power Sources 145:30
15. Pathapati PR, Xue X, Tang J (2005) Renew Energy 30:1
16. Jones PB, Lakeman JB, Mepsted GO et al (1999) J Power Sources 80:242
17. Hottinen T, Mikkola M, Lund P (2004) J Power Sources 129:68
18. Ziegler C, Yu HM, Sundmacher JO (2005) J Electrochem Soc 152A:1555
19. Hamelin J, Agbossou K, Laperrière A et al (2001) Int J Hydrog Energy 26:625
20. Amphlett JC, de Oliveira EH, Mann RF et al (1997) J Power Sources 65:173
21. Williams KA, Keith WT, Marcel MJ et al (2007) J Power Sources 163:971
22. Schenck ME, Lai J-S, Stanton K (2005) Ann IEEE Appl Power Electron Conf Expo 1:114
23. Lasia A (1999) In: Conway BE, Bockris JOM, White RE (eds) Modern aspects of electrochemistry, vol 32. Kluwer Academic/Plenum Publishers, New York
24. Weydahl H, Møller-Holst S, Hagen G et al (2007) J Power Sources 171:321
25. Newman J, Thomas-Alyea KE (2004) Electrochemical systems, 3rd edn. Wiley, Hoboken, New Jersey
26. Fraser SD, Hacker V (2008) J Appl Electrochem 38:451
27. Kim J, Lee SM, Srinivasan S (1995) J Electrochem Soc 142:2670

28. Squadrito G, Maggio G, Passalacqua E, Lufrano F, Patti A (1999) J Appl Electrochem 29:1449
29. Pisani L, Murgia G, Valentini M, D'Aguanno B (2002) J Power Sources 108:192
30. Fouquet N, Doulet C, Nouillant C, Dauphin-Tanguy G, Ould-Bouamamab B (2006) J Power Sources 159:905
31. Boillot M, Bonnet C, Jatroudakis N, Carre P, Didierjean S, Lapicque F (2006) Fuel Cells 6:31
32. Boillot M, Bonnet C, Didierjean S, Lapicque F (2007) J Appl Electrochem 37:103
33. Ciureanu M, Mikhailenko SD, Kaliaguine S (2003) Catal Today 82:195
34. Yuan X, Wang H, Sun JC, Zhang J (2007) Int J Hydrog Energy 32:4365
35. Xie Z, Holdcroft S (2004) J Electroanal Chem 568:247
36. Malevich D, Halliop E, Peppley BA, Pharoah JG, Karana K (2009) J Electrochem Soc 156:B216
37. Liu YX, Murphy MW, Baker DR, Gu WB, Ji CC, Jorne J, Gasteiger HA (2009) J Electrochem Soc 156:B970